Lab on a Chip

PAPER

Cite this: *Lab Chip*, 2018, **18**, 371

Linking invasive motility to protein expression in single tumor cells†

Jung-Ming G. Lin, [ab] Chi-Chih Kang,[b] Yun Zhou,[c] Haiyan Huang,[cde] Amy E. Herr [ab] and Sanjay Kumar*[abf]

Received 19th September 2017,
Accepted 18th December 2017

DOI: 10.1039/c7lc01008g

rsc.li/loc

The invasion of malignant cells into tissue is a critical step in the progression of cancer. While it is increasingly appreciated that cells within a tumor differ in their invasive potential, it remains nearly unknown how these differences relate to cell-to-cell variations in protein expression. Here, we introduce a microfluidic platform that integrates measurements of invasive motility and protein expression for single cells, which we use to scrutinize human glioblastoma tumor-initiating cells (TICs). Our live-cell imaging microdevice is comprised of polyacrylamide microchannels that exhibit tissue-like stiffness and present chemokine gradients along each channel. Due to intrinsic differences in motility, cell subpopulations separate along the channel axis. The separated cells are then lysed *in situ* and each single-cell lysate is subjected to western blotting in the surrounding polyacrylamide matrix. We observe correlations between motility and Nestin and EphA2 expression. We identify protein–protein correlations within single TICs, which would be obscured with population-based assays. The integration of motility traits with single-cell protein analysis – on the same cell – offers a new means to identify druggable targets of invasive capacity.

Solid tumors consist of cell subpopulations that differ widely in gene and protein expression, tumor-forming ability, chemoresistance, and invasive capacity.[1,2] Over the past decade, this notion has been formalized into the cancer stem cell (a.k.a. tumor-initiating cell) paradigm, which argues that tumor initiation, progression, and metastasis are driven by a rare-cell cohort whose properties are masked by population measurements.[3,4] Consequently, such population-based measurements can obscure the understanding of cancer development, progression, and response to treatment. An important hallmark of cancer progression is the invasion of tumor cells into the surrounding tissue and, in some cases, metastasis to distant sites.[5,6] However, little is definitively known about how the invasive phenotype (or potential) relates to protein expression within a single cell.[5,7]

The precision afforded by microfluidics tools allows the scrutiny of tumor invasion potential with more nuanced and higher-dimensionality descriptors than population-based assays.[4,8–11] However, the vast majority of these approaches have focused entirely on the functional characterization of single-cell motility, with few efforts to connect single-cell migration with specific marker expression.[4,10] In one such study, cell speed was measured within one microfluidic channel device while expression of motility-relevant mRNAs for the same cell was subsequently measured using molecular beacons in a separate device.[4] However, mRNA levels are neither fully predictive of protein expression nor capable of reporting protein signaling events that occur after translation.[12]

For single-cell protein detection, the *de facto* standard is immunocytochemistry (ICC). While useful, ICC suffers from fixation artifacts (limiting specificity), background antibody cross-reactivity (impacting multiplexing and increasing background signal), and the challenge of accurately measuring total fluorescence intensity from a cell volume.[13,14] On the other hand, standard slab western blot detects much improved protein quantification but requires pooled populations of cells and is therefore unsuitable for single-cell analysis. To achieve the best of both approaches, the Herr Laboratory has recently developed the single-cell western blot (scWB) assay, which can quantify protein levels in ~10^3 separate cells within 4 h, with a lower limit of detection of ~27 000 copies of a protein.[15] We have successfully used this assay to investigate heterogeneity in cell signaling, differentiation and chemotherapeutic resistance in specific cell lines.[15–18] In addition to acting as both a molecular sieve and blotting membrane, the polyacrylamide (PA) gel used to

[a] *UC-Berkeley-UCSF Graduate Program in Bioengineering, University of California, Berkeley, CA 94720, USA. E-mail: skumar@berkeley.edu*
[b] *Department of Bioengineering, University of California, Berkeley, CA 94720, USA*
[c] *Division of Biostatistics, School of Public Health, University of California, Berkeley, CA 94720, USA*
[d] *Department of Statistics, University of California, Berkeley, CA 94720, USA*
[e] *Center for Computational Biology, University of California, Berkeley, CA 94720, USA*
[f] *Department of Chemical and Biomolecular Engineering, University of California, Berkeley, CA 94720, USA*

† Electronic supplementary information (ESI) available. See DOI: 10.1039/c7lc01008g

create the scWB has the potential to be micropatterned with features that integrate important, complementary cellular measurements, including single-cell resolution motility assays.

Here, we describe an integrated microfluidic device that combines the scWB assay with live-cell imaging of invasive cell motility (Fig. 1), which we term SCAMPR (**S**ingle-**C**ell **A**nalysis of **M**otility and **Pr**oteotype). In this platform, cells are induced to chemotactically migrate along microchannels and imaged to capture instantaneous and time-averaged cellular migratory properties (*i.e.*, speed, persistence and aspect ratio) for later quantification. Each cell is then lysed *in situ*, with the lysate electrophoresed through the wall of the channel and size-separated due to molecular sieving through the PA gel, photoimmobilized to the PA gel (*via* light-activated benzophenone methacrylamide co-monomer),[18] and then immunoprobed to quantify candidate proteins. Using the SCAMPR platform, we first separate cell populations with known differences in motility. We then investigate the correlation of protein levels with migratory behavior in primary glioblastoma tumor-initiating cell (GBM TIC) cultures. SCAMPR represents an important step towards the identification of tumor-specific proteomic predictors of invasive motility, relevant to questions spanning basic discovery to precision medicine.

Materials and methods

Antibodies

Antibodies employed for the migratory scWB study include rabbit anti-EphA2[19,20] (1 : 10, 6997S, Cell Signaling, with anti-rabbit secondary antibody conjugated with Alexa-Fluor 647), mouse anti-STAT3[21,22] (1 : 10, 9139S, Cell Signaling, with anti-mouse secondary antibody conjugated with Alexa-Fluor 488), mouse anti-Nestin[23,24] (1 : 10, MAB5326, EMD-Millipore, with anti-mouse secondary antibody conjugated with Alexa-Fluor 488), rabbit anti-β-tubulin[17,25] (1 : 10, ab6046, Abcam, with anti-rabbit secondary antibody conjugated with Alexa-Fluor 647).

Cell culture

U373 Empty Vector and U373 DN Rac1 GBM cell lines[26] were maintained at 37 °C in a 5% CO_2 humidified chamber and cultured in high glucose DMEM (Life Technologies) supplemented with 10% calf serum (JR Scientific), 100 U mL^{-1} penicillin, 100 μg mL^{-1} streptomycin, 1× MEM non-essential amino acids, and 1 mM sodium pyruvate (Life Technologies). To induce gene expression, 25 ng mL^{-1} doxycycline was added to the cell culture medium 48 h prior to any experiments. As a technical note, we used U373 cells from the American Type Culture Collection (ATCC). U373 cells have

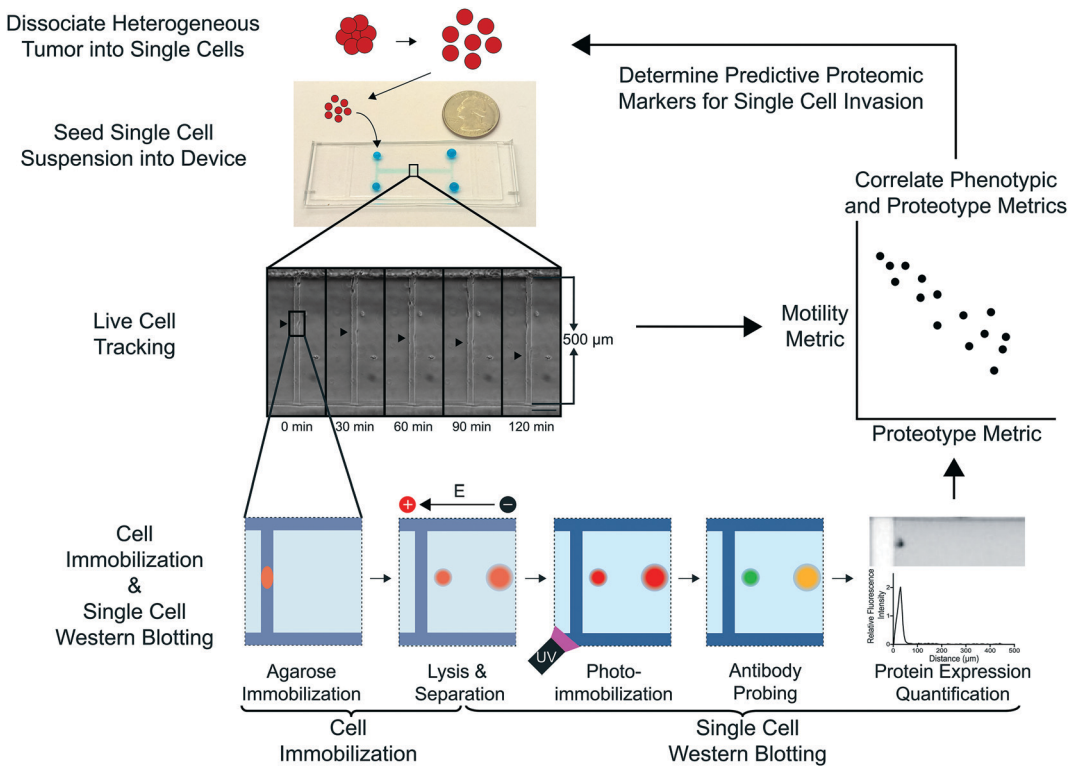

Fig. 1 Microfluidic integration supports a Single-Cell Analysis of Motility and Proteotype (SCAMPR) assay. A heterogeneous population of primary cells is first dissociated into a single-cell suspension. The cells are then seeded into the SCAMPR device and tracked as each cell chemotactically migrates through the channels under a chemokine gradient, which reports motility and motility-related parameters, persistence and average aspect ratio. Immediately following the live-cell tracking, cells are immobilized in an agarose layer and the scWB is run in order to measure protein expression on each tracked cells. Motility and proteotype information from single cells are then correlated to associate proteomic markers with invasive motility properties.

recently been recognized to be a subclone of the human glioblastoma line U251, with the two lines having subsequently diverged to exhibit differential drug sensitivities.[27] Cell lines were authenticated using short tandem repeat analysis and tested negative for mycoplasma.

The primary GBM TIC line L0 was originally obtained from Dr. Brent Reynolds' laboratory at the University of Florida and has been described in an earlier study.[28] L0 gliomaspheres were propagated in growth conditions with serum-free medium (Neurocult NS-A Proliferation kit, Stem Cell Technologies) supplemented with epidermal growth factor (20 ng mL^{-1}, R&D Systems), basic fibroblast growth factor (R&D Systems) and 2 mg mL^{-1} heparin (Sigma-Aldrich) The gliomaspheres were serially passaged every 5–7 days, when the spheres reached a diameter of ~150 μm. Gliomaspheres were dissociated with trypsin/ethylenediaminetetraacetic acid (0.05%) (Gibco) for 2 min and then replated in fresh media with the addition of epidermal growth factor, basic fibroblast growth factor, and heparin.

Polyacrylamide gel layer silicon wafer fabrication

The PA gel layer silicon master was fabricated in a two-step process using standard lithography techniques (Fig. S1†). The silicon wafer was first pre-cleaned with piranha solution (3 : 1 sulfuric acid to hydrogen peroxide), washed with water, and briefly baked to remove any residual water. A 15 μm layer of SU-8 2010 (Microchem, Boston, MA) was spin-coated onto the wafer and photopatterned with the "migratory microchannel photomask". After the post exposure bake, a 50 μm layer of SU-8 2025 (Microchem, Boston, MA) was spin-coated onto the existing SU-8 layer and photopatterned with the "gradient-generating channel photomask". After another post-exposure bake, the wafer was developed and hard baked. The final wafer was coated with dimethyldichloromethylsilane (Sigma-Aldrich) to prevent the PA gel from adhering to the wafer. Detailed information on the silicon master fabrication is listed in the ESI.†

Polyacrylamide gel layer fabrication

The PA base gel layer used for the protein separations was fabricated as detailed previously.[15,18] The PA gel precursor (8% T, 3.3% C acrylamide/bisacrylamide (Sigma-Aldrich), 3 mM BPMAC (Pharm-Agra Laboratories)) was polymerized using 0.08% APS and 0.2% TEMED (Sigma-Aldrich).[16] scWB slides were functionalized with sulfo-SANPAH (Thermo Scientific) and then with either 40 μg mL^{-1} fibronectin (Millipore) in PBS (U373) or 100 μg mL^{-1} laminin (Invitrogen) in serum-free media (GBM TICs).

Polyacrylamide gel stiffness measurements

AFM indentation measurements were performed as described earlier[29] using pyramid-tipped probes (OTR4, Bruker AFM Probes) and fitting force curves with a modified Hertz model.

PDMS layer fabrication

Sylgard 184 base and curing agent was mixed in a 10 : 1 ratio and degassed. The resulting solution was degassed and poured into a rectangular mold to a height of 1.5 mm. The PDMS was then cured at 80 °C for 2 h. After the PDMS was cured, rectangular slabs (3 cm (L) × 7.5 cm (W)) were cut out of the mold. 3 mm diameter holes that match the inlet and outlet wells on the PA gel were then punched out of the PDMS rectangular slab.

SCAMPR device fabrication and seeding

The micropatterned PA gel was first incubated in appropriate medium for at least 1 h prior to device fabrication. Following incubation, the gel was removed and the excess liquid was aspirated away. The PDMS lid was gently placed on top of the PA gel, with the holes in the PDMS aligned to the inlet and outlet microwell patterns on the PA gel. The hybrid PDMS/PA device was then placed under vacuum (200 mmHg) in a vacuum desiccator (Bel-Art) for 6 min to reversibly seal the layers together. After the vacuum step, cell culture media was placed in both inlet ports and allowed to equilibrate in the device.

To seed the device, any excess medium was first aspirated from all four inlet and outlet microwells. Then a 30 μl aliquot of cell suspension (1 million cells mL^{-1}) was added to the top inlet port. Due to the pressure differences, cells flow into and lodge at the start of the migratory microchannels. The cells were then allowed to adhere prior to chemokine gradient formation and imaging (1 h for GBM TICs or 2 h for U373s).

SCAMPR cell motility separation assay

For the proof of principle cell motility separation assay, U373 Empty Vector cells were loaded with 5 μM CMFDA Cell Tracker dye (Thermo Fisher Scientific) and U373 DN Rac1 cells were pre-loaded with 5 μM CMPTX Cell Tracker dye (Thermo Fisher Scientific) per the manufacturer's instructions. The two cell lines were mixed in a 1 : 1 ratio and a 30 μL aliquot of the mixed cell suspension (1 million cells mL^{-1}) was seeded into the device. After 2 h, the device was imaged with FITC and TRITC filter cubes, in order to determine the starting locations of the cells within the channels. Then 30 μL of U373 media and U373 media containing 20 μg mL^{-1} SDF-1 were placed in opposing inlet ports. The aliquots were refreshed every 2 h for a 10 h period. After 10 h, the device was again imaged to determine the final location of the cells.

Stage 1 of the SCAMPR assay

Live-cell imaging was performed using a Nikon Ti-E2000-E2 microscope equipped with a motorized, programmable stage (Applied Scientific Instrumentation), an incubator chamber to maintain constant temperature, humidity, and CO_2 levels (*In vivo* Scientific), a digital camera (Photometrics Coolsnap

HQ2), and NIS Elements (Nikon Instruments Inc.) software. Images were taken at 5 ms exposure, 2 × 2 pixel binning using a 10×-objective (Nikon CFI Plan Fluor DLL 10×).

Stages 2 and 3 of the SCAMPR assay

The second and third stage of the SCAMPR assay consists of nine steps: (1) the PDMS lid was gently removed; (2) liquid agarose, 5% w/v in PBS, (Life Technologies) at 40 °C was poured directly onto the PA gel layer and allowed to set for 10 min at room temperature. Liquid agarose was stirred continuously prior to pouring onto the PA gel; (3) the *in situ* cell lysis was performed by directly pouring the lysis buffer (12 mM Tris/96 mM glycine pH 8.3 buffer (Bio-Rad) containing 0.5% w/v SDS (Sigma-Aldrich), 0.1% v/v Triton X-100 (Thermo Fisher), and 0.25% w/v sodium deoxycholate (Sigma-Aldrich)) over the agarose-covered slide and cell lysis was allowed to proceed for 15 s; (4) lysate was analyzed *via* PA gel electrophoresis (E = 40 V cm^{-1}, I = 81–95 mA) for 15 s; (5) protein bands were immobilized by UV activation of the benzophenone. UV light was generated using a UV mercury arc lamp (Lightningcure LC5, Hamamatsu) and directed through a Lumatec series 380 liquid light guide with inline UV filter (300–380 nm bandpass XD1001, Omega Optical) suspended approximately 10 cm above the slide. PA gels were exposed for 45 s with UV power at the slide surface of ~40 mW (cm^2)$^{-1}$; (6) the agarose layer was melted away by submerging the agarose covered slide in PBS and heating the PBS to 70 °C; (7) the SCAMPR slides were probed with primary and fluorescent secondary antibodies. Slides were first incubated with a primary antibody diluted in TBST (Santa Cruz Biotechnology, sc-281695) supplemented with 2% Bovine Serum Albumin (BSA) (A730, Sigma-Aldrich) for 3 h. Slides were then washed for 30 min in TBST, and then incubated with the appropriate fluorescently labeled secondary diluted in TBST supplemented with 2% BSA for 1 h. Slides were washed again for 30 min in TBST and dried under a nitrogen stream; (8) the slides were scanned with a fluorescence microarray scanner with 450 PMT gain 100% power. STAT3 expression was measured with 450 PMT gain and 100% power. EphA2 expression was measured with 650 PMT gain and 100% power. β-Tubulin expression was measured with 650 PMT gain and 100% power. All scans had a spatial resolution of 5 μm. Detection of Alexa Fluor 488 and Alexa Fluor 647 labeled secondary antibodies was performed using 488 nm and 635 nm lasers, respectively. Emission filters for the 488 nm spectral channel were from Omega Optical (XF3405) and for the 635 nm channel, a built-in far-red emission filter was used; (9) a region of interest "lane" was then used to segment the protein signals. The protein signal intensity profiles were background-subtracted and to Gaussian curves with a minimum signal-to-noise (SNR) of 3 and R^2 threshold of 0.7. Protein expression was calculated by summing the area under the curve (AUC) of the Gaussian curve. An overview of the steps is presented in Fig. 1.

Measurement of cell motility parameters

Following a previously established protocol,[29] we measured GBM TIC motility using 10× phase contrast time-lapse images acquired every 15 min over a 2 h period. ImageJ software (NIH) was used to track the centroid of each cell from one frame to another to yield instantaneous migration speeds, which were then averaged over the entire time course of the experiment to yield the migration speed of a cell. Persistence was calculated by measuring the distance between the initial and final position and dividing by the total path length. The aspect ratio was calculated by dividing the major axis length of the cell by the minor axis length of the cell for each frame in the time-lapse and averaging the values for all the frames. The aspect ratio of a cell was not calculated if the entire outline of the cell was not observed. Cells that were observed to be sticking to each other were also excluded from analysis.

Imaging of single-cell lysis

GBM TICs were first labeled with 5 μM CMFDA dye (Thermo Fisher Scientific) per the manufacturer's instructions. Cells were then seeded into a microwell at the terminus of the enclosed SCAMPR devices and allowed to adhere for at least 1 h. Next, the PDMS lid was removed and the device was either left in PBS (open condition) or layered with a 100 μm thick 5% w/v agarose layer (Agarose condition) (Life Technologies). The device was then placed in a custom lysis chamber with an optically transparent bottom to allow for imaging. Lysis buffer was poured over the device and images were taken every 0.5 seconds for 60 seconds. Time-lapse imaging was taken using MetaMorph software (Molecular Devices) with a 200 ms exposure time, at 1 × 1 pixel binning through a 10× magnification objective (Olympus UPlan FLN, NA 045) on an Olympus IX71 inverted fluorescence microscope equipped with an camera (Photometrics CoolSNAP HQ2), motorized stage (Applied Scientific Instrumentation), FITC/GFP filter cube (Omega XF100-3, Ex/Em: 445–495/505–575 nm), and shuttered mercury lamp light source (X-cite, Lumen Dynamics).

Immunocytochemistry

After removing the PDMS lid, the SCAMPR slide was washed with PBS and fixed with 4% paraformaldehyde (Alfa Aesar) in PBS. Slides were then washed 3 times with PBS and then permeabilized for 15 min with 0.5% v/v Triton X-100 in PBS. Slides were again washed 3 times with PBS and then blocked for 1 h at room temperature with 5% v/v goat serum (Thermo Fisher Scientific) in PBS. The blocking buffer was then aspirated and then the slides were incubated with 1 : 200 mouse anti-human Nestin (Millipore) overnight at 4 °C in staining buffer (1% v/v goat serum in PBS). After 3 washes of staining buffer, the slides were incubated in 1 : 500 goat anti-mouse IgG, Alexa Fluor 546 (Thermo Fisher Scientific) and Hoechst 33342 (Thermo Fisher Scientific) in staining buffer for 1 h at room temperature. After the secondary incubation, the slides were washed with PBS and stored in PBS at 4 °C prior to imaging.

ICC images were captured using an inverted Nikon Ti-E microscope equipped with a motorized stage (Prior Scientific, Inc.), a digital camera (Roper Scientific) and NIS Elements (Nikon Instruments, Inc) software. Images were taken with a 500 ms exposure time, 1 × 1 pixel binning through a 10× magnification objective (Nikon CFI Plan Fluor DLL 10×). A TRITC filter cube (Nikon G-2E/C, Ex/Em: 528–553/590–650 nm) and DAPI filter cube (Nikon UV-2E/C, Ex/Em: 340–380/435–485 nm) were used to detect the Nestin-Alexa Fluor 546 signal and Hoechst stain, respectively. ImageJ software (NIH) was used to measure total fluorescence of a cell by creating a region of interest around the cell, measuring the total integrated intensity, and then subtracting the background total integrated intensity.

Flow cytometry

TICs were stained with PE anti-EphA2 antibody (356803, Biolegend) according to manufacturer's instructions. TICs were then sorted with a BD Influx cell sorter into the top 5% and bottom 5% EphA2 expression level subpopulations. Immediately after sorting, the sorted subpopulations were seeded into the SCAMPR device for live cell tracking.

Statistical analysis

All statistical studies except for the Canonical Correlation Analysis and Pearson's correlation analysis were performed in Prism (Prism 7). All Spearman correlations were reported with two-tailed *p*-values. The results from Mann–Whitney tests and Welch's *t*-tests were reported with two-tailed *p*-values. Brown-Forsythe's test was used to determine non-equivalence of variance in marker expression in each motility category. The D'Agostino-Pearson omnibus normality test was used to determine normality of populations.

A custom R script was used to first perform the canonical correlation analysis and then calculate the Pearson's correlation between each of the variables and canonical components. We used a permutation test to determine the *p*-value for the largest canonical correlation. Keeping the phenotype profile of every cell as is, we randomly permuted the protein expression files across the cells to generate a random mapping between phenotypes and proteins for each cell and derived an empirical null distribution for the largest canonical correlation between phenotypes and proteins. Under the null hypothesis, no strong canonical correlation should be found between phenotypes and proteins.

For all statistical tests, results with p values less than 0.05 were considered significant. Details of comparisons and replicates are provided in the appropriate figure legends.

Results

Design and operation of the SCAMPR device

We designed, fabricated, and validated a microdevice that measures both (i) cellular migration parameters and (ii) protein expression for individual cells within a population of cells. To make these dual measurements on the same cell, the SCAMPR platform comprises a planar polyacrylamide microfluidic device housing microtrenches that are enclosed to form microchannels using a polydimethylsiloxane (PDMS) lid. The assay completes in three stages. In the first assay stage, the device presents mechanical and chemical cues to migrating tumor cells in microfluidic channels. Intrinsic cell-to-cell differences in motility spatially resolve cells within the channels. In the second assay stage, we replace the PDMS lid with an agarose layer to both immobilize the separated cells and to minimize lysate loss (by convection) during in-channel chemical lysis. Finally, in the third assay stage, the device supports a single-cell western blot (scWB) in the surrounding PA gel, yielding proteotypic information for each cell. By combining these three assay stages, migratory parameters such as speed, persistence, and cell aspect ratio are correlated with protein expression to link the invasive motility phenotype to proteotype for an individual cell.

To fabricate the SCAMPR device, microtrenches were first cast in a PA gel and then enclosed using a PDMS lid to form microchannels (Fig. S1a†). The PA gel presents a stiffness within the range of vascular basement membrane (30 kPa as measured by AFM)[30] and also functions as the protein sieving matrix during subsequent electrophoretic analysis of each single-cell lysate. Along the axis of each microchannel, we create a chemokine concentration gradient using a source-sink design.[9] The PDMS lid facilitates long-term live-cell imaging, which is aided by the fact that PDMS is optically clear, non-cytotoxic, and supports gas exchange with the ambient environment.[31] To integrate the motility assay with the scWB assay, we transiently sealed the PDMS lid to the PA gel using a vacuum pulse, allowing for lid delamination prior to subsequent scWB steps (Fig. S1b†).

SCAMPR stage 1: validation of chemokine gradient for cell separation

We first sought to characterize the chemokine gradient in the SCAMPR device. Chemotactic motility is an important feature of tumor invasion *in vivo*, and the chemotactic machinery is being actively explored as a source of new drug targets in cancer.[32–34] To create stable chemokine gradients in the SCAMPR device, we implemented a source-sink design.[9] We characterized the linearity and reproducibility of the chemokine gradients using FITC-dextran as a surrogate for stromal cell-derived factor 1 (SDF-1), which is known to drive GBM invasion *in vivo*.[35,36] We introduced 30 μl of PBS containing 10 μg mL^{-1} 10 kDa FITC-dextran in the inlet port in one gradient-generating channel and 30 μl of PBS in the inlet port of the opposing channel. By replacing each solution every 2 h and imaging the device every hour, we observed a relatively stable linear average concentration gradient over a 10 h period (R^2 = 0.996; coefficient of variation (CV) = 14.6%, n = 33 curves from 3 devices) (Fig. 2a). We also observed relatively consistent performance in gradient generation and maintenance across multiple devices (average intra-device CV = 10.8% with a standard deviation of 8.6%, n = 3; intra-device

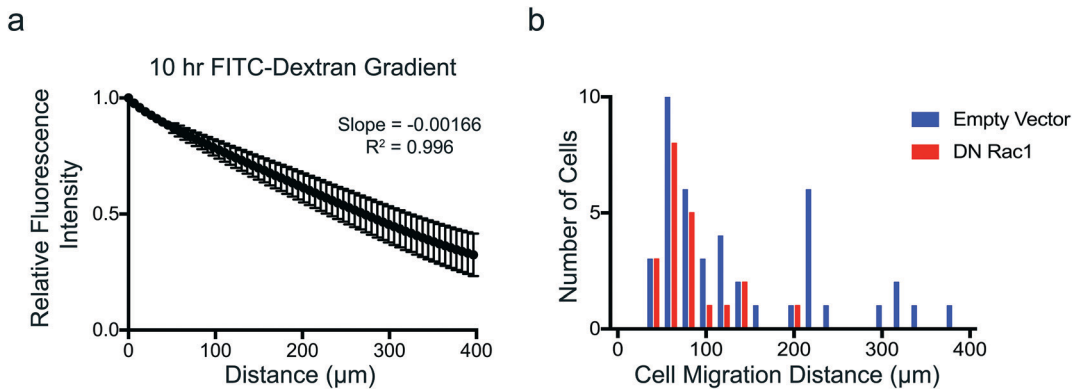

Fig. 2 SDF-1 chemokine gradient resolves two cell lines with known differences in motility. a) Time-averaged FITC-dextran fluorescence signal in the SCAMPR device. Linear regression of average gradient shows a slope of −0.00166 RFU per μm and a R^2 value of 0.996. The average gradient curve is calculated from 33 gradients from 3 separate devices. Error bars represent standard deviation calculated from 33 gradients from 3 separate devices. RFU: relative fluorescence unit. b) Migration-induced separation of a mixed population of labeled Empty Vector and DN Rac1 cell lines. Empty vector: 43 cells from 3 independent experiments; DN Rac1: 23 cells from 3 independent experiments.

CV calculated from the gradients during the 10 h period) (Fig. S2†).

Next, we tested the ability of an SDF-1 gradient to separate two labeled cell populations with known population-level differences in motility. We utilized U373 human glioma cells stably transduced with a dominant negative mutant of Rac1 (DN Rac1) and a matched line transduced with a non-coding empty vector (Empty Vector). Rac1 plays a role in lamellipodial protrusion and contributes strongly to invasion and metastasis,[37] and depletion of Rac1 or overexpression of a dominant negative Rac1 mutant has been reported to reduce glioma cell invasiveness and survival.[37] We first verified that the Empty Vector and DN Rac1 cell lines exhibit the expected population-level differences in motility with empty vector cells migrating significantly faster than the DN Rac1 cells on a fibronectin coated glass surface (Fig. S3,† Welch's *t*-test, $p < 0.0001$, $n = 33$ and 23 for empty vector and DN Rac1, respectively).

We then loaded DN Rac1 and Empty Vector cells with CMPTX and CMFDA CellTracker dye respectively, mixed the two cell populations in an equal ratio, and introduced them into our device. After 10 h, the fastest Empty Vector cell migrated 380 μm into the microchannel compared to 200 μm for the fastest DN Rac1 cell (Fig. 2b). Furthermore, we observed twelve Empty Vector cells that are highly migratory in the microchannels compared to the entire DN Rac1 population ($n = 23$ cells). Thus, we are able to utilize the SCAMPR assay to resolve subpopulations of cells according to chemotactic motility.

SCAMPR stage 2: characterization of cell immobilization and lysis

We then sought to incorporate scWB measurements into our chemotactic migration platform. The major hurdle in performing the three-stage SCAMPR assay in an open-microchannel format is protein dilution during cell lysis due to rapid diffusive and convective loss. We reasoned that we could limit this loss by physically encasing the cells within a buffer-permeable solid matrix prior to electrophoresis. For this purpose, we chose agarose, which transitions from a molten liquid to a solid gel upon cooling and decreases the diffusivity of proteins and creates quiescent fluid conditions.[38] To introduce the agarose layer, we first removed the PDMS lid and covered the device with molten agarose. After the agarose solidified, lysis buffer (12 mM Tris/96 mM glycine pH 8.3 buffer containing 0.5% w/v sodium dodecyl sulfate (SDS), 0.1% v/v Triton X-100, and 0.25% w/v sodium deoxycholate) was applied to the agarose, thus chemically lysing the now-immobilized cells.

To understand the impact of the agarose encapsulating layer (Agarose condition) on lysate retention, we loaded cells with a fluorescent cytoplasmic protein labeling dye, chemically lysed the cells within the microchannels, and tracked lysate fluorescence over time (Fig. 3a). We characterized lysate dilution using total integrated signal intensity and signal width ($w = 4\sigma$; with σ extracted from a Gaussian fit). We observed a 72% increase in total integrated signal intensity in the Agarose condition compared to the Open condition ($n = 3$ cells for both conditions) at the 15 s time-point, which represents our optimized lysis time for GBM TICs (Fig. 3b). Furthermore, at the 15 s time-point, we observed an 84% reduction in signal peak width in the Agarose condition relative to the Open condition, which improves the likelihood of achieving single-cell resolution during electrophoresis and blotting by preventing cellular lysate from neighboring cells from mixing (Fig. 3c, d). Thus, the Agarose condition mitigates single-cell lysate dilution more effectively than the Open condition, thereby facilitating the subsequent scWB.

SCAMPR stage 3: integration of scWB

Having tracked cell motility and controlled cell lysis in the SCAMPR device, we then applied the SCAMPR device to scrutinize a population of classical subtype GBM TICs derived from a patient tumor (Video S1†). TICs are a stem-like

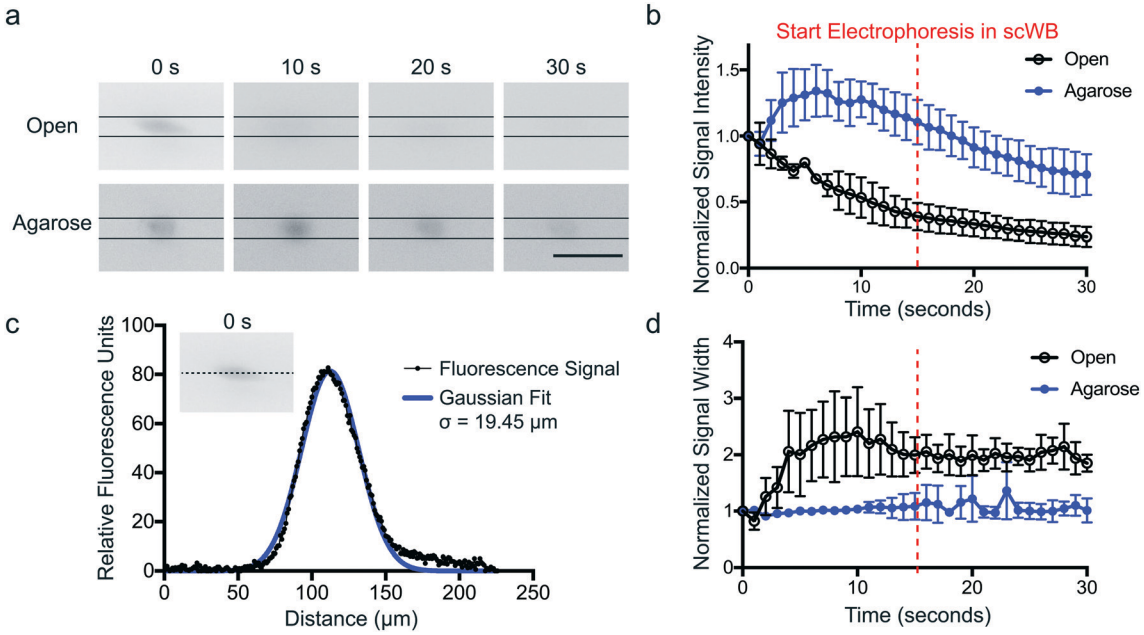

Fig. 3 Agarose cell-encapsulation reduces dilution of single-cell lysates. a) Representative images of fluorescently labeled GBM TICs during in-microchannel lysis with (Agarose) and without (Open) an agarose encapsulating layer. TICs were labeled with CMFDA cell tracker dye. Lines were added to indicate the edges of the microchannel. Scale bar = 20 μm. b) Time course of the total integrated fluorescence signal from labeled GBM TICs lysed in the Open and Agarose conditions. At the start of electrophoresis (indicated by the red line), the Agarose condition improved lysate retention by 72% relative to the Open condition. Error bars represent standard deviation calculated from 3 independent experiments. c) Representative fluorescence signal (black) of a cell at the beginning of lysis (0 s) and the corresponding Gaussian fit line (blue) with the σ value shown. The dashed line in the insert denotes the axis of the fluorescence signal. d) Time course of the normalized peak width quantified from the fitted Gaussian curve of the fluorescence intensity. At the start of the electrophoresis at 15 s, the Agarose condition shows an 84% decrease in peak width compared to the Open condition. Error bars represent standard deviation calculated from 3 independent experiments.

subpopulation of GBM cells that drives tumor growth and recurrence, therapeutic resistance, and, of most relevance to the studies reported here, invasion and seeding of secondary tumors *in vivo*.[29]

We first analyzed two motility-relevant parameters of GBM TICs in the SCAMPR device: persistence and average cell aspect ratio. We defined persistence as the net displacement of the cell divided by the total path length travelled during a set interval. Previous studies on 2D substrates have shown a positive correlation of these two parameters with cell speed.[39,40] We first observed a mean TIC speed of 81 μm h^{-1} (minimum speed of 7.4 μm h^{-1}, maximum speed of 170 μm h^{-1}, n = 68 cells, n = 9 devices) in the SCAMPR microchannels, which is faster than previously reported values of this TIC line on 2D PA substrates (Fig. 4a).[29] Throughout the time-lapse, we did not observe any cells transitioning to a persisting, rounded morphology, which is an early indication of cell death. We then applied Spearman's rank-order

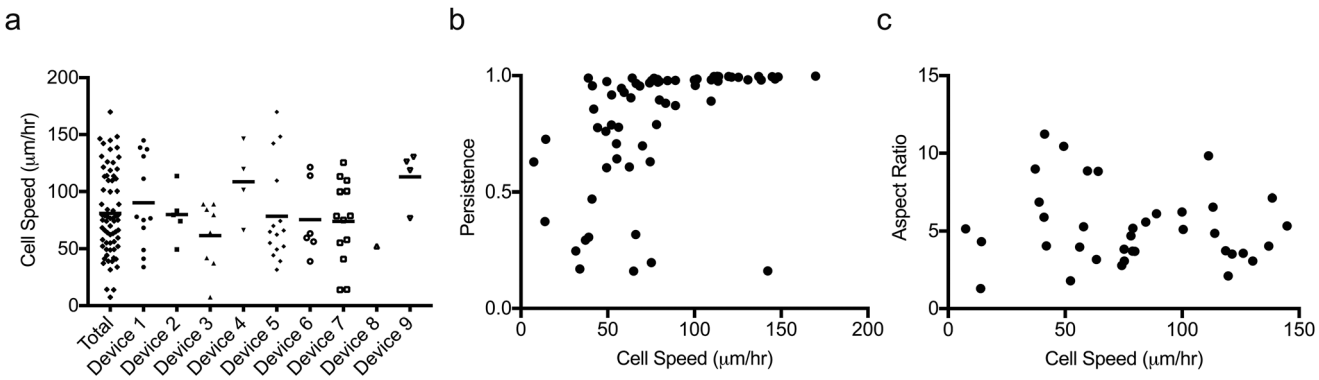

Fig. 4 Persistence, but not aspect ratio, is correlated with TIC speed in the SCAMPR device. a) Dot plot showing the individual TIC speeds across 9 devices for a GBM TIC line. Each point represents a single cell, with a global maximum TIC speed of ~170 μm h^{-1} and a global minimum of 7.4 μm h^{-1}. Lines represent the mean TIC speed per device. Scatter plots reveal that the TIC persistence (b), but not average aspect ratio (c) is significantly correlated with TIC speed (Spearman's rank $r_{Persistence}$ = 0.676, $p < 0.0001$, n = 68 cells; $r_{Aspect\ Ratio}$ = −0.134, p = 0.430, n = 37 cells).

correlation to investigate if persistence and average cell aspect ratio correlated with TIC speed in the SCAMPR device. Although we observed the expected positive correlation of persistence and speed (Spearman's rank $r = 0.676$, $p < 0.0001$, $n = 64$ cells) (Fig. 4b), we did not observe a similar trend with aspect ratio and speed (Spearman's rank $r = -0.133$, $p = 0.430$, $n = 37$ cells) (Fig. 4c), which may result in part from our use of 2D images to quantify 3D objects. Additionally, we observed the same trends when we ranked the parameters (persistence, aspect ratio) and correlated the ranks of these parameters with the rank of the cell speed for each individual TIC (Spearman's rank $r_{\text{Persistence}} = 0.664$, $p < 0.0001$, $n = 64$; $r_{\text{Aspect Ratio}} = -0.134$, $p = 0.430$, $n = 37$ cells) (Fig. S4†).

We then screened The Cancer Genome Atlas (TCGA) dataset for specific markers relevant to TIC function and upregulated in GBMs relative to normal brain. We analyzed the RNA expression levels of Nestin, EphA2, STAT3, and β-tubulin in the classical subtype of GBM tumors. Nestin, EphA2, and STAT3 have been previously shown to be essential for the survival and tumorigenicity of GBM cells.[41–47] In addition to being a TIC marker, EphA2 has been shown to promote invasiveness and correlate with tumor stage and progression.[42] Similarly, STAT3 has been shown to regulate TIC growth and self-renewal, and downregulation of STAT3 leads to decreased motility and invasion.[44,48] β-Tubulin is an important component of the microtubule network, which is a common target in chemotherapy (*e.g.* paclitaxel).[49,50]

Our TCGA analysis revealed that all four of these markers are significantly upregulated in GBM tissue relative to normal brain (Mann–Whitney test, $p < 0.001$ for all 4 markers, Nestin: $n = 11$, 54 for normal brain and GBM, respectively; STAT3: $n = 11$, 54 for normal brain and GBM, respectively; EphA2: $n = 11$, 54 for normal brain and GBM, respectively; β-tubulin: $n = 10$, 53 for normal brain and GBM, respectively) (Fig. S5†). Further analysis of the TCGA data set for marker correlations revealed significant correlations only between EphA2 and Nestin and between STAT3 and β-tubulin RNA expression (Spearman's rank $r_{\text{EphA2–Nestin}} = 0.395$, $p = 0.004$, $n = 52$ tumors; $r_{\text{STAT3–Nestin}} = -0.062$, $p = 0.661$, $n = 52$ tumors; $r_{\text{β-tubulin–Nestin}} = 0.220$, $p = 0.113$, $n = 53$ tumors; $r_{\text{EphA2–STAT3}} = -0.019$, $p = 0.894$, $n = 53$ tumors; $r_{\text{β-tubulin–STAT3}} = 0.303$, $p = 0.027$, $n = 53$ tumors; $r_{\text{β-tubulin–EphA2}} = 0.006$, $p = 0.961$, $n = 53$ tumors) (Fig. S6†). Furthermore, we observed the same significant correlations when we ranked and correlated the RNA expression levels for each marker (Spearman's rank $r_{\text{EphA2–Nestin}} = 0.398$, $p = 0.004$, $n = 52$ tumors; $r_{\text{STAT3–Nestin}} = -0.142$, $p = 0.317$, $n = 52$ tumors; $r_{\text{β-tubulin–Nestin}} = 0.219$, $p = 0.116$, $n = 53$ tumors; $r_{\text{EphA2–STAT3}} = -0.019$, $p = 0.894$, $n = 53$ tumors; $r_{\text{β-tubulin–STAT3}} = 0.303$, $p = 0.028$, $n = 53$ tumors; $r_{\text{β-tubulin–EphA2}} = -0.005$, $p = 0.974$, $n = 53$ tumors) (Fig. S7†).

The TCGA correlations are based on population-level analysis of patient biopsies and do not account for cell-to-cell differences in marker expression, which has been shown to contribute strongly to disease progression and therapeutic response.[51–54] We therefore applied our SCAMPR assay to ask whether these marker correlations, on the protein level, persist within individual GBM TICs.

To measure single-cell protein expression, we utilized the third stage of the SCAMPR assay, the scWB. After lysis of the agarose-immobilized cells, an electric field is applied and the single-cell lysate electromigrates into the surrounding PA gel, where the proteins are sized by electrophoretic mobility. A brief pulse of UV light is applied to the SCAMPR device and the proteins in the PA gel slab are covalently immobilized to benzophenone methacrylamide incorporated in the PA gel. The bound proteins are then probed with primary target-specific antibodies and fluorescent secondary antibodies to allow for visualization and quantification. Since we visualize the location of single cells within the device, we normalize protein expression on a per cell basis (Fig. 5a).

In contrast to the TCGA correlation results, the SCAMPR assay reported a significant correlation between β-tubulin with Nestin (Spearman's rank $r = 0.503$, $p = 0.002$, $n = 34$ cells). STAT3 exhibits a strong correlation with both β-tubulin and Nestin, with the p-values being close to statistically significant ($r_{\text{STAT3–β-tubulin}} = 0.361$, $p = 0.0545$, $n = 29$ cells; $r_{\text{STAT3–Nestin}} = 0.293$, $p = 0.056$, $n = 43$ cells). That is, the three proteins Nestin, STAT3, and β-tubulin have relatively high pairwise correlations between each other. EphA2, however, was reported to have weak or no correlations with those three proteins (Spearman's rank $r_{\text{EphA2–Nestin}} = 0.352$, $p = 0.118$, $n = 21$ cells; $r_{\text{EphA2–STAT3}} = 0.269$, $p = 0.265$, $n = 19$ cells; $r_{\text{EphA2–β-tubulin}} = 0.453$, $p = 0.069$, $n = 17$ cells) (Fig. 5b). Similarly, ranking and correlating the SCAMPR protein expression values revealed the same trends (Spearman's rank $r_{\text{EphA2–Nestin}} = -0.352$, $p = 0.118$, $n = 21$ cells; $r_{\text{STAT3–Nestin}} = 0.295$, $p = 0.055$, $n = 43$ cells; $r_{\text{β-tubulin–Nestin}} = 0.503$, $p = 0.002$, $n = 34$ cells; $r_{\text{EphA2–STAT3}} = 0.263$, $p = 0.276$, $n = 19$ cells; $r_{\text{β-tubulin–STAT3}} = 0.362$, $n = 0.054$, $n = 29$ cells; $r_{\text{β-tubulin–EphA2}} = 0.453$, $n = 0.069$, $n = 17$ cells) (Fig. S8†).

Furthermore, the multiparametric assay allows correlation of motility with protein expression for each individual cell studied. To contextualize protein expression variation with respect to motility, we classified TICs into one of three motility categories (low motility: 0–56.6 μm h^{-1}, medium motility: 56.6–113.3 μm h^{-1}, high motility: 113.3–170 μm h^{-1}) with motility categories defined based on three equally sized intervals of speed ranging from 0 to 170 μm h^{-1} (maximum TIC speed). We compared the variance in Nestin, STAT3, EphA2, and β-tubulin expression for each motility category (Fig. 5b). We observed a difference in the variation of β-tubulin expression among different motility subpopulations but not the other three markers across the motility categories (Brown–Forsythe's test, $p = 0.037$, $n = 11$, 15, 8 cells for low, medium, and high motility subpopulations, respectively).

Linking motility to protein expression

The results above suggest that while multiple proteins are overexpressed in invasive tumors at the population level, only

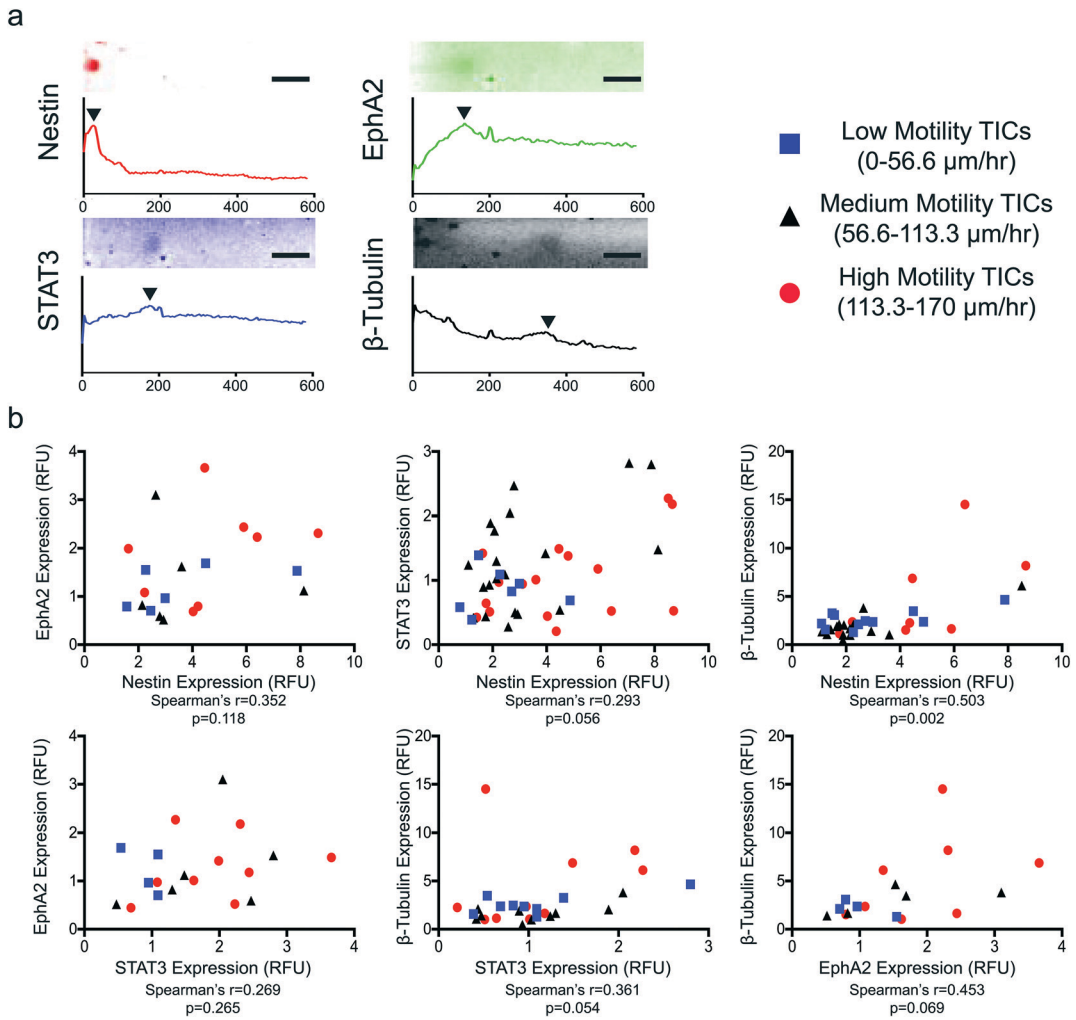

Fig. 5 SCAMPR assay reveals novel protein expression correlations in GBM TICs. a) Representative fluorescence micrographs and intensity plots from the scWB assay of GBM TICs. Arrows indicate peak location. Scale bars represent 100 μm. b) Biaxial scatter plots report protein expression for all markers for each GBM TICs from low, medium and high motility TIC subpopulations. Motility subpopulations were created based on three equally sized intervals of speed ranging from 0 μm h^{-1} to 170 μm h^{-1} (maximum observed TIC speed). TICs were binned into motility subpopulations based on magnitude of speed (low motility: 0–56.6 μm h^{-1}, medium motility: 56.6–113.3 μm h^{-1}, high motility: 113.3–170 μm h^{-1}). Blue squares, black triangles and red circles represent low, medium and high motility subpopulations, respectively.

a subset of these proteins is associated with the propensity of individual TICs to invade. Because such proteins could conceivably serve as novel druggable targets to slow invasion, we sought to identify specific proteins that correlate with high invasive motility in GBM TICs. Previous studies suggest that Nestin regulates tumor growth and invasion at the population level.[41] Therefore, we hypothesized that Nestin expression and motility would be correlated in individual GBM TICs.

We performed the three-stage SCAMPR assay on the TICs and observed a positive correlation between Nestin expression and cell speed, which is consistent with literature observations (Spearman's rank $r = 0.381$, $p = 0.001$, $n = 68$ cells) (Fig. 6a).[55,56] We also observed a similar positive correlation when comparing the rank of Nestin expression and the rank of cell speed (Spearman's rank $r = 0.383$, $p = 0.001$, $n = 68$ cells) (Fig. S9a†). Interestingly, parallel ICC assays in which we fixed, permeabilized, and immunostained TICs after removing the PDMS lid but before adding agarose did not reveal a significant correlation between Nestin expression and cell speed (Spearman's rank $r = 0.053$, $p = 0.696$, $n = 56$ cells) (Fig. S10†). We hypothesize that differences in SCAMPR and ICC results could be due to the previously mentioned shortcomings (fixation artifacts, antibody cross-reactivity, and quantifying total fluorescence in 3D) with ICC, which may prevent the detection of subtle trends in protein expression.

As previously mentioned, multiplexed protein detection is supported by the SCAMPR device, which compares expression of multiple proteins within the same cell. Protein multiplexing is useful when assessing correlation between marker expression and cell motility characteristics. Given the roles of EphA2, STAT3, and β-tubulin in TIC invasion, we next sought to understand the relationship between these markers and TIC motility. We observed a positive correlation of EphA2

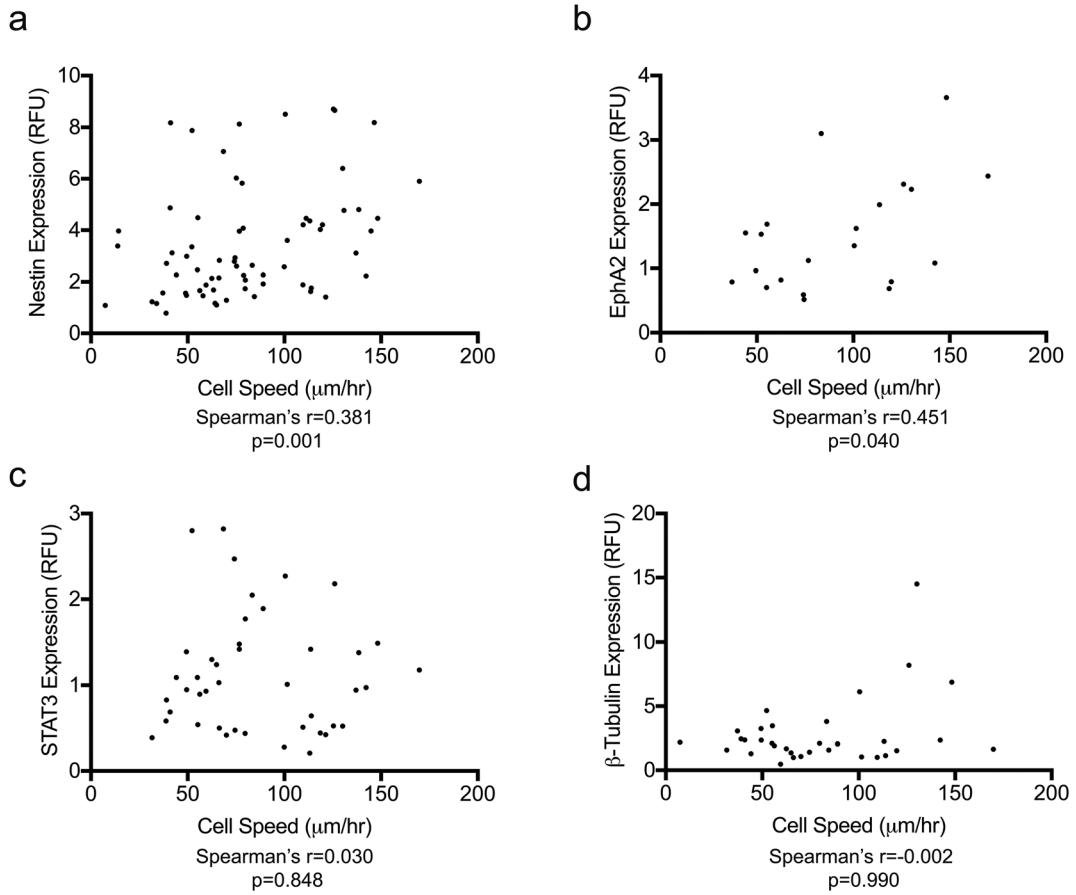

Fig. 6 SCAMPR assay reveals Nestin and EphA2 correlate with TIC speed. Scatter plots of individual TICs show that (a) Nestin and (b) EphA2 are positively correlated with TIC speed (Spearman's rank r_{Nestin} = 0.381, p = 0.001, n = 68 cells; r_{EphA2} = 0.451, p = 0.040, n = 21 cells). However, (c) STAT3 and (d) β-tubulin are not correlated with TIC speed (Spearman's rank r_{STAT3} = 0.030, p = 0.848, n = 43 cells; $r_{β\text{-tubulin}}$ = −0.002, p = 0.990, n = 34 cells).

and cell speed (Spearman's rank r = 0.451, p = 0.040, n = 21 cells), thus corroborating other studies that have shown EphA2 can drive TIC behaviors including growth and self-renewal (Fig. 6b).[42] We further validated the EphA2 correlation by sorting the TICs into low and high EphA2 expression level subpopulations, seeding both subpopulations into separate SCAMPR devices, and quantifying the single-cell motilities of each subpopulation in the SCAMPR device. As expected, we observed a significantly higher average motility in the high EphA2 expression subpopulation compared to the low EphA2 expression subpopulation (Mann–Whitney test, $p < 0.0001$, n = 18, 24 for the low and high EphA2 subpopulations, respectively) (Fig. S11†)

On the other hand, SCAMPR did not detect a correlation between STAT3 or β-tubulin and cell speed (Spearman's rank r_{STAT3} = 0.030, p = 0.848, n = 43 cells; $r_{β\text{-tubulin}}$ = −0.002, p = 0.990, n = 34 cells) (Fig. 6c and d). The lack of a correlation for STAT3 reflects the results of other studies that have shown that the phosphorylation, not the expression, of STAT3 is necessary to activate downstream pathways and dictate cellular phenotypes.[43] We also observed the same trends when we correlated the ranks of these three proteins with the rank of cell speed (Spearman's rank r_{EphA2} = 0.451, p = 0.040, n = 21 cells; r_{STAT3} = 0.031, p = 0.0842, n = 43 cells; $r_{β\text{-tubulin}}$ = −0.001, p = 0.997, n = 34 cells) (Fig. S9b–d†).

Joint analysis of SCAMPR metrics

Having scrutinized protein–protein and protein–motility correlations, we performed joint analysis of TIC phenotypes and proteotypes. We first generated single-cell proteotypic profiles using the multiplexed SCAMPR assay (Nestin, STAT3, EphA2, β-tubulin). Then, by mapping the motility information onto the proteotypic profiles, we identified proteotype profiles that describe low or high motility TICs (Fig. 7a). We then performed canonical correlation analysis (CCA) on the phenotypic variables (speed, persistence, and aspect ratio) and a log2 transformation of protein expression values. CCA provides a useful way to relate two sets of variables (*e.g.*, phenotypes and proteins) and determine commonalities amongst the two sets; it finds linear combinations of the variables of each set that have maximum correlation with each other. We utilized the log2 transformation of the protein expression

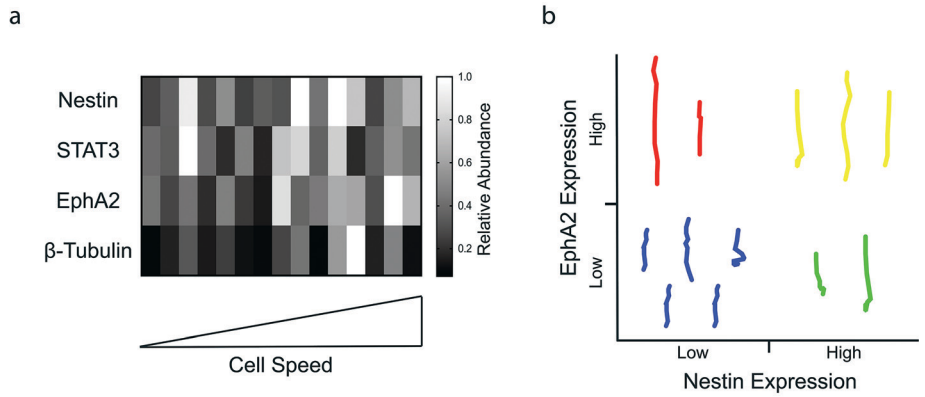

Fig. 7 SCAMPR assay allows for joint multivariable analysis of phenotype and proteotype. a) Relative expression levels of Nestin, EphA2, STAT3, and β-tubulin in single GBM TICs with respect to cell speed. Only the subset of TICs with quantifiable expression levels for all four proteins is displayed in this plot. Protein expression in each TIC is normalized to the strongest signal for each protein. Within each row, tile color corresponds to relative expression level with black being the lowest and white being the highest. Each column represents the proteotype for one TIC and the TICs are organized in increasing cell speed order. b) Representative cell trajectories of single TICs expressing either low or high Nestin or EphA2. Trajectories represent total path length over 2 h. High and low expression levels represent the top 50% and bottom 50% expression level for each respective protein.

values to bring the magnitude of the protein expression values closer to the phenotypic values. CCA and post-hoc Pearson's correlation showed that Nestin positively correlates with speed and persistence, with speed being more relevant than persistence to the first canonical component of the phenotype variables (1st canonical correlation $r = 0.48$, $p < 0.05$) (Fig. S12†). By further utilizing the multiplexing capability of the SCAMPR device and probing for more targets, we would increase the accuracy of the invasive proteotypic profiles.

Additionally, since we have the TIC position data (used to calculate motility), we then investigated the relationship between protein expression and TIC total path length (Fig. 7b). We plotted representative paths for TICs with low or high expression of Nestin or EphA2, which both correlated with motility. We first observed that the TICs in the high Nestin/high EphA2 quadrant show longer path lengths than the TICs in the low Nestin/low EphA2 quadrant, which is consistent with the previously observed protein–motility correlations. We also observed that TICs in the other quadrants (low Nestin/high EphA2, high Nestin/low EphA2) displayed varied trajectory lengths. This result highlights the heterogeneity in motility behavior for TICs, even in specific subpopulations defined by expression levels for two different proteins.

Discussion

The invasion of individual tumor cells into tissue is a defining feature of cancer. However, it is unclear how the expression of specific proteins drives or predicts the invasive phenotype of single tumor cells. While single-cell RNA sequencing is beginning to lend important insight into cell-to-cell variations in gene expression within tumors,[57] the bulk of our current knowledge is based on population analyses such as RNA sequencing and western blotting. Perhaps even more importantly, contemporary single-cell approaches do not readily allow for cell-by-cell correlation of proteotype with phenotype. Here, we have developed an integrated microfluidic device (SCAMPR) to correlate phenotypic information with multiple protein expression levels from the same single cell. Using the SCAMPR device, we first discovered a correlation of Nestin and β-tubulin within our GBM TIC line, which could not have been deduced from inter-tumor data sets. We further discovered that while Nestin and EphA2 expression positively correlate with migration speed, STAT3 and β-tubulin expression show no correlation with cellular migration speed. These results highlight the unique ability of the SCAMPR device in identifying correlations within a single patient-derived cell line, which offers an eventual route for precision medicine based on patient-specific identification of proteins that slow invasion in tissue-like microenvironments. Furthermore, our results represent some of the first single-cell protein expression studies in TICs that correlate protein expression with phenotypic traits.

Our approach has the potential to address a number of important gaps left by the TCGA and other large-scale data sets. For example, these data sets do not, in general, permit analysis of protein cross-correlations within a single tumor cell. Utilizing our platform, we discovered that, within a GBM TIC population, β-tubulin expression correlates with Nestin expression, a prognostic marker of tumor malignancy.[46] This observation suggests that a similar analysis will lead to the identification of other important but yet undiscovered targets. Additionally, by investigating a wide range of targets, we can identify multiple, correlated proteins and, in turn, key signaling networks that can be targeted as a unit. The observation of this correlation highlights the importance of single-cell technologies, such as our platform, in complementing existing large-scale data sets, such as the TCGA.

Similarly, correlation of cell phenotype and proteotype at a single-cell level validates and complements results from population-based assays. Specifically, in GBM TICs, we identified that Nestin and EphA2 expression positively correlate

with cell speed, which agrees with previously published results.[41,58] At the same time, by utilizing the multiplexing capability of the platform, we also observed that Nestin and EphA2 expression levels do not correlate with each other. Taken together, these two results suggest that, even within a single population, there are multiple proteotypic profiles that describe highly motile GBM TICs. Should these two proteins causally drive motility, one would need to target both Nestin and EphA2, not only one of the targets, to limit the highly motile subpopulation.

Since our platform identified Nestin and EphA2 as positive predictors of TIC motility, analysis of a panel of GBM lines from different subtypes is an intriguing future direction. These studies could determine whether Nestin and EphA2 serve as universal GBM TIC motility predictors or if these two proteins are a subtype or tumor-specific phenomenon. Additionally, the investigation of additional proteins and phospho-proteins would be valuable towards sharpening the motility-proteotype profiles. While 4 protein targets were measured per cell in this study (*i.e.*, coarse-grained signatures, Fig. 7a), exploring a broader range of targets should reduce this granularity. Doing so should also facilitate identification of additional novel intra-tumor protein correlations.

The SCAMPR platform investigates motility and protein expression in a fraction of the cell population loaded into the device. Cells that successfully lodge at the head of microchannel are assayed. All other cells are discarded. As bulk fluid flow is used to introduce the cells, we posit that localization to the microchannel head is a random process. Consequently, cell-to-cell variation in invasive motility is assessed for a sub-set of dissociated tumor cells. Methods for actively localizing cells to the head of the microchannel system are of interest for further platform development. For example, optical tweezer technology has been previously used to manipulate single cells from one microfluidic platform to another one[4] and this technology could be used to place single cells at the head of each microchannel.

In addition to the active localization of cells, stable chemokine gradient generation is another important area of platform advancement. As mentioned previously, there exists variations in the chemokine gradient with our current experimental setup (average intra-device CV = 10.8% with a standard deviation of 8.6%, $n = 3$; intra-device CV calculated from the gradients during the 10 h period) and we are investigating other methods to decrease this variation, including continuous infusion of source and sink materials. However, it is important to note that although the changes in gradient intensity may alter the "resolution" with which we can separate cells according to motility, there is no reason to believe these variations in gradient will affect the order in which cells exit the channel – *i.e.*, cells deemed "fast" and "slow" relative to one another in a 1× chemokine gradient will still be so in a 2× chemokine gradient. This is supported by Fig. 2b, in which we resolved differences in migration between two cell lines with known differences in population level motility. Despite device-to-device variations in the chemokine gradient, the Empty Vector cells (high motility) still migrated further into the channel compared to the DN Rac1 cells (low motility).

While we have focused on GBM invasive motility, the SCAMPR device could be used to study the invasion process in other cancer types.[17] The SCAMPR device could also be modified to incorporate physical features of the tumor microenvironment, such as three-dimensional matrices. In addition to lending new fundamental insight into the cellular basis of motility, invasion, and metastasis, such devices could also serve as the basis for discovery and screening platforms, analogous to tissue-on-chip systems.[59]

Conclusions

We report on a microfluidic platform that integrates measurements of invasive motility and protein expression with single-cell resolution. By developing a corresponding workflow that includes a method to transiently seal two layers of PDMS and PA together, we successfully identified and validated proteins that correlate with invasive motility in a single patient-derived GBM cell line, which is significant step forward in elucidating markers that dictate cell-to-cell differences in GBM invasive potential. We envision that this technology will prove valuable for the identification of patient specific proteins that regulate invasion, thereby establishing a platform for future diagnostic technologies.

Conflicts of interest

There are no conflicts to declare.

Acknowledgements

We thank members of the Kumar and Herr laboratory at UC Berkeley for feedback and discussion. This work was supported by the National Institutes of Health (1R21CA174573 to S. K. and A. E. H.; 5R21EB019880 to A. E. H.; T32GM098218 training grant support to J. G. L), the W.M. Keck Foundation (Science and Engineering Grant to S. K.), and the Cancer Research Coordinating Committee (fellowship to J. G. L.).

References

1 G. H. Heppner and B. E. Miller, Tumor heterogeneity: biological implications and therapeutic consequences, *Cancer Metastasis Rev.*, 1983, **2**, 5–23.

2 A. Marusyk and K. Polyak, Tumor heterogeneity: Causes and consequences, *Biochim. Biophys. Acta, Rev. Cancer*, 2010, **1805**, 105–117.

3 J. Lathia, S. Mack, E. Mulkearns-Hubert, C. Valentim and J. Rich, Cancer stem cells in glioblastoma, *Genes Dev.*, 2015, **29**, 1203–1217.

4 D. Gallego-Perez, L. Chang, J. Shi, J. Ma, S. H. Kim and X. Zhao, *et al.* On-Chip Clonal Analysis of Glioma-Stem-Cell Motility and Therapy Resistance, *Nano Lett.*, 2016, **16**, 5326–5332.

5 P. Friedl and S. Alexander, Cancer invasion and the microenvironment: Plasticity and reciprocity, *Cell*, 2011, **147**, 992–1009.

6 M. Mak, C. Reinhart-King and D. Erickson, Elucidating mechanical transition effects of invading cancer cells with a subnucleus-scaled microfluidic serial dimensional modulation device, *Lab Chip*, 2013, **13**, 340–348.

7 S. Kumar and V. M. Weaver, Mechanics, malignancy, and metastasis: The force journey of a tumor cell, *Cancer Metastasis Rev.*, 2009, **28**, 113–127.

8 A. Pathak and S. Kumar, Independent regulation of tumor cell migration by matrix stiffness and confinement, *Proc. Natl. Acad. Sci. U. S. A.*, 2012, **109**, 10334–10339.

9 Z. Tong, E. M. Balzer, M. R. Dallas, W. C. Hung, K. J. Stebe and K. Konstantopoulos, Chemotaxis of cell populations through confined spaces at Single-Cell resolution, *PLoS One*, 2012, **7**, 1–10.

10 Y.-C. Chen, S. G. Allen, P. N. Ingram, R. Buckanovich, S. D. Merajver and E. Yoon, Single-cell Migration Chip for Chemotaxis-based Microfluidic Selection of Heterogeneous Cell Populations, *Sci. Rep.*, 2015, **5**, 9980.

11 P. K. Chaudhuri, M. Ebrahimi Warkiani, T. Jing, K. Kenry and C. T. Lim, Microfluidics for research and applications in oncology, *Analyst*, 2016, **141**, 504–524.

12 C. Huang, J. Cao, K. J. Huang, F. Zhang, T. Jiang and L. Zhu, *et al.* Inhibition of STAT3 activity with AG490 decreases the invasion of human pancreatic cancer cells in vitro, *Cancer Sci.*, 2006, **97**, 1417–1423.

13 J. C. Waters, Accuracy and precision in quantitative fluorescence microscopy, *J. Cell Biol.*, 2009, **185**, 1135–1148.

14 K. A. Yamauchi and A. E. Herr, Subcellular western blotting of single cells, *Microsyst. Nanoeng.*, 2017, **3**, 16079.

15 A. J. Hughes, D. P. Spelke, Z. Xu, C.-C. Kang, D. V. Schaffer and A. E. Herr, Single-cell western blotting, *Nat. Methods*, 2014, **11**, 749–755.

16 C. C. Kang, J. M. G. Lin, Z. Xu, S. Kumar and A. E. Herr, Single-cell western blotting after whole-cell imaging to assess cancer chemotherapeutic response, *Anal. Chem.*, 2014, **86**, 10429–10436.

17 E. Sinkala, E. Sollier-Christen, C. Renier, E. Rosas-Caynelles, J. Che and K. Heirich, *et al.* Profiling protein expression in circulating tumour cells using microfluidic western blotting, *Nat. Commun.*, 2017, **8**, 14622.

18 T. A. Duncombe, C. Kang, S. Maity, T. M. Ward, M. D. Pegram and N. Murthy, *et al.* Hydrogel Pore-Size Modulation for Enhanced Single-Cell Western Blotting, *Adv. Mater.*, 2016, **28**, 327–334.

19 M. S. Zahari, X. Wu, B. G. Blair, S. M. Pinto, R. S. Nirujogi and C. A. Jelinek, *et al.* Activating Mutations in PIK3CA Lead to Widespread Modulation of the Tyrosine Phosphoproteome, *J. Proteome Res.*, 2015, **14**, 3882–3891.

20 O. Eriksson, Å. Thulin, A. Asplund, G. Hegde, S. Navani and A. Siegbahn, Cross-talk between the Tissue Factor / coagulation factor VIIa complex and the tyrosine kinase receptor EphA2 in cancer, *BMC Cancer*, 2016, **16**, 341.

21 C. Yu, Q. Zhan and Y. Song, Migfilin Protein Promotes Migration and Invasion in Human Glioma through Epidermal Growth Factor Receptor-mediated Phospholipase C- and STAT3 Protein Signaling Pathways, *J. Biol. Chem.*, 2012, **287**, 32394–32405.

22 Y. Zhou, S. Wu, C. Liang, Y. Lin, Y. Zou and K. Li, *et al.* Transcriptional upregulation of microtubule-associated protein 2 is involved in the protein kinase A-induced decrease in the invasiveness of glioma cells, *Neuro-Oncology*, 2015, **17**, 1578–1588.

23 S. Duan, G. Yuan, X. Liu, R. Ren, J. Li and W. Zhang, *et al.* PTEN deficiency reprogrammes human neural stem cells towards a glioblastoma stem cell-like phenotype, *Nat. Commun.*, 2015, **6**, 10068.

24 L. Cheng, W. Hu, B. Qiu, J. Zhao, Y. Yu and W. Guan, *et al.* Generation of neural progenitor cells by chemical cocktails and hypoxia, *Cell Res.*, 2014, **24**, 665–679.

25 D. J. Johann, J. Rodriguez-Canales, S. Mukherjee, A. P. DaRue, J. C. Hanson and M. Emmert-Buck, *et al.* Approaching solid tumor heterogeneity on a cellular basis by tissue proteomics using laser capture microdissection and biological mass spectrometry, *J. Proteome Res.*, 2009, **8**, 2310–2318.

26 J. L. MacKay, A. Sood and S. Kumar, Three-dimensional patterning of multiple cell populations through orthogonal genetic control of cell motility, *Soft Matter*, 2014, **10**, 2372.

27 A. A. Stepanenko and V. M. Kavsan, Karyotypically distinct U251, U373, and SNB19 glioma cell lines are of the same origin but have different drug treatment sensitivities, *Gene*, 2014, **540**, 263–265.

28 L. P. Deleyrolle, A. Harding, K. Cato, F. A. Siebzehnrubl, M. Rahman and H. Azari, *et al.* Evidence for label-retaining tumour-initiating cells in human glioblastoma, *Brain*, 2011, **134**, 1331–1343.

29 S. Y. Wong, T. A. Ulrich, L. P. Deleyrolle, J. L. MacKay, J. M. G. Lin and R. T. Martuscello, *et al.* Constitutive activation of myosin-dependent contractility sensitizes glioma tumor-initiating cells to mechanical inputs and reduces tissue invasion, *Cancer Res.*, 2015, **75**, 1113–1122.

30 J. A. Wood, S. J. Liliensiek, P. Russell, P. F. Nealey and C. J. Murphy, Biophysical cueing and vascular endothelial cell behavior, *Materials*, 2010, **3**, 1620–1639.

31 G. M. Whitesides, The origins and the future of microfluidics, *Nature*, 2006, **442**, 368–373.

32 T. Kitamura and J. W. Pollard, Therapeutic potential of chemokine signal inhibition for metastatic breast cancer, *Pharmacol. Res.*, 2015, **100**, 266–270.

33 H. Yamaguchi, J. Wyckoff and J. Condeelis, Cell migration in tumors, *Curr. Opin. Cell Biol.*, 2005, 559–564.

34 E. T. Roussos, J. S. Condeelis and A. Patsialou, Chemotaxis in cancer, *Nat. Rev. Cancer*, 2011, **11**, 573–587.

35 A. Rape, B. Ananthanarayanan and S. Kumar, Engineering strategies to mimic the glioblastoma microenvironment, *Adv. Drug Delivery Rev.*, 2014, **79**, 172–183.

36 Y. Zhou, P. H. Larsen, C. Hao and V. W. Yong, CXCR4 is a major chemokine receptor on glioma cells and mediates their survival, *J. Biol. Chem.*, 2002, **277**, 49481–49487.

37 M. Nakada, S. Nakada, T. Demuth, N. L. Tran, D. B. Hoelzinger and M. E. Berens, Molecular targets of glioma invasion, *Cell. Mol. Life Sci.*, 2007, **64**, 458–478.

38 E. M. Johnson, D. A. Berk, R. K. Jain and W. M. Deen, Hindered diffusion in agarose gels: Test of effective medium model, *Biophys. J.*, 1996, **70**, 1017–1023.

39 P. Maiuri, J. F. Rupprecht, S. Wieser, V. Ruprecht, O. Bénichou and N. Carpi, *et al.* Actin flows mediate a universal coupling between cell speed and cell persistence, *Cell*, 2015, **161**, 374–386.

40 A. S. Meyer, S. K. Hughes-Alford, J. E. Kay, A. Castillo, A. Wells and F. B. Gertler, *et al.* 2D protrusion but not motility predicts growth factor-induced cancer cell migration in 3D collagen, *J. Cell Biol.*, 2012, **197**, 721–729.

41 T. Ishiwata, K. Teduka, T. Yamamoto, K. Kawahara, Y. Matsuda and Z. Naito, Neuroepithelial stem cell marker nestin regulates the migration, invasion and growth of human gliomas, *Oncol. Rep.*, 2011, **26**, 91–99.

42 E. Binda, A. Visioli, F. Giani, G. Lamorte, M. Copetti and K. L. Pitter, *et al.* The EphA2 Receptor Drives Self-Renewal and Tumorigenicity in Stem-like Tumor-Propagating Cells from Human Glioblastomas, *Cancer Cell*, 2012, **22**, 765–780.

43 M. M. Sherry, A. Reeves, J. K. Wu and B. H. Cochran, STAT3 is required for proliferation and maintenance of multipotency in glioblastoma stem cells Maureen, *Stem Cells*, 2009, **27**, 2383–2392.

44 F. Chen, Y. Xu, Y. Luo, D. Zheng, Y. Song and K. Yu, *et al.* Down-regulation of Stat3 decreases invasion activity and induces apoptosis of human glioma cells, *J. Mol. Neurosci.*, 2010, **40**, 353–359.

45 J. Neradil and R. Veselska, Nestin as a marker of cancer stem cells, *Cancer Sci.*, 2015, **106**, 803–811.

46 R. H. Dahlrot, S. Hansen, S. S. Jensen, H. D. Schrøder, J. Hjelmborg and B. W. Kristensen, Clinical value of CD133 and nestin in patients with glioma: A population-based study, *Int. J. Clin. Exp. Pathol.*, 2014, **7**, 3739–3751.

47 Y. H. Ma, R. Mentlein, F. Knerlich, M. L. Kruse, H. M. Mehdorn and J. Held-Feindt, Expression of stem cell markers in human astrocytomas of different WHO grades, *J. Neuro-Oncol.*, 2008, **86**, 31–45.

48 M. Priester, E. Copanaki, V. Vafaizadeh, S. Hensel, C. Bernreuther and M. Glatzel, *et al.* STAT3 silencing inhibits glioma single cell infiltration and tumor growth, *Neuro-Oncology*, 2013, **15**, 840–852.

49 A. J. Terzis, F. Thorsen, O. Heese, T. Visted, R. Bjerkvig and O. Dahl, *et al.* Proliferation, migration and invasion of human glioma cells exposed to paclitaxel (Taxol) in vitro, *Br. J. Cancer*, 1997, **75**, 1744–1752.

50 A. Panopoulos, M. Howell, R. Fotedar and R. L. Margolis, Glioblastoma motility occurs in the absence of actin polymer, *Mol. Biol. Cell*, 2011, **22**, 2212–2220.

51 N. J. Szerlip, A. Pedraza, D. Chakravarty, M. Azim, J. McGuire and Y. Fang, *et al.* Intratumoral heterogeneity of receptor tyrosine kinases EGFR and PDGFRA amplification in glioblastoma defines subpopulations with distinct growth factor response, *Proc. Natl. Acad. Sci. U. S. A.*, 2012, **109**, 3041–3046.

52 A. Soeda, A. Hara, T. Kunisada, S. Yoshimura, T. Iwama and D. M. Park, The evidence of glioblastoma heterogeneity, *Sci. Rep.*, 2015, **5**, 7979.

53 S. Bao, Q. Wu, R. E. McLendon, Y. Hao, Q. Shi and A. B. Hjelmeland, *et al.* Glioma stem cells promote radioresistance by preferential activation of the DNA damage response, *Nature*, 2006, **444**, 756–760.

54 H. S. Phillips, S. Kharbanda, R. Chen, W. F. Forrest, R. H. Soriano and T. D. Wu, *et al.* Molecular subclasses of high-grade glioma predict prognosis, delineate a pattern of disease progression, and resemble stages in neurogenesis, *Cancer Cell*, 2006, **9**, 157–173.

55 W. Kleeberger, G. S. Bova, M. E. Nielsen, M. Herawi, A. Y. Chuang and J. I. Epstein, *et al.* Roles for the stem cell-associated intermediate filament nestin in prostate cancer migration and metastasis, *Cancer Res.*, 2007, **67**, 9199–9206.

56 Y. Matsuda, Z. Naito, K. Kawahara, N. Nakazawa, M. Korc and T. Ishiwata, Nestin is a novel target for suppressing pancreatic cancer cell migration, invasion and metastasis, *Cancer Biol. Ther.*, 2011, **11**, 512–523.

57 A. P. Patel, I. Tirosh, J. J. Trombetta, A. K. Shalek, M. Shawn and H. Wakimoto, *et al.* Single-cell RNA-seq highlights intratumoral heterogeneity in primary glioblastoma, *Science*, 2014, **344**, 1396–1401.

58 U. Gopal, J. E. Bohonowych, C. Lema-Tome, A. Liu, E. Garrett-Mayer and B. Wang, *et al.* A novel extracellular Hsp90 mediated co-receptor function for LRP1 regulates EphA2 dependent glioblastoma cell invasion, *PLoS One*, 2011, **6**, 1–14.

59 A. Guan, P. Hamilton, Y. Wang, M. Gorbet, Z. Li and K. S. Phillips, Medical devices on chips, *Nat. Biomed. Eng.*, 2017, **1**, 45.

